

RESEARCH ARTICLE

Open Access



A versatile mouse model to advance human microglia transplantation research in neurodegenerative diseases

Lutgarde Serneels^{1†}, Annerieke Sierksma^{1†}, Emanuela Pasciuto^{2†}, Ivana Geric¹, Arya Nair¹, Anna Martinez-Muriana¹, An Snellinx¹ and Bart De Strooper^{1,3*}

Abstract

Background Recent studies highlight the critical role of microglia in neurodegenerative disorders, and emphasize the need for humanized models to accurately study microglial responses. Human-mouse microglia xenotransplantation models are a valuable platform for functional studies and for testing therapeutic approaches, yet currently those models are only available for academic research. This hampers their implementation for the development and testing of medication that targets human microglia.

Methods We developed the *hCSF1^{Bdes}* mouse line, which is suitable as a new transplantation model and available to be crossed to any disease model of interest. The *hCSF1^{Bdes}* model created by CRISPR gene editing is RAG2 deficient and expresses human CSF1. Additionally, we crossed this model with two humanized *App* KI mice, the *App^{Hu}* and the *App^{SAA}*. *Flow cytometry, immunohistochemistry and bulk sequencing was used to study the response of microglia in the context of Alzheimer's disease.*

Results Our results demonstrate the successful transplantation of iPSC-derived human microglia into the brains of *hCSF1^{Bdes}* mice without triggering a NK-driven immune response. Furthermore, we confirmed the multipronged response of microglia in the context of Alzheimer's disease. The *hCSF1^{Bdes}* and the crosses with the Alzheimer's disease knock-in model *App^{SAA}* and the humanized *App* knock-in control mice, *App^{Hu}* are deposited with EMMA and fully accessible to the research community.

Conclusion The *hCSF1^{Bdes}* mouse is available for both non-profit and for-profit organisations, facilitating the use of the xenotransplantation paradigm for human microglia to study complex human disease.

Keywords Mouse xenotransplantation model, Microglia, Alzheimer's disease

[†]Lutgarde Serneels, Annerieke Sierksma, Emanuela Pasciuto, and Ivana Geric contributed equally to this work.

*Correspondence:

Bart De Strooper
bart.destrooper@kuleuven.be

¹ VIB Center for Brain and Disease Research and Department of Neurosciences, KU Leuven, Louvain, Belgium

² VIB Center for Molecular Neurology and Department of Biomedical Sciences, University of Antwerp, Antwerp, Belgium

³ Dementia Research Institute, University College London, London, UK



Background

Roughly 5–10% of our brain cells are microglia [31], yet despite their relatively small number, they are indispensable for proper brain function. These yolk-sac derived brain-resident macrophages undertake a variety of critical functions, including brain surveillance for invading pathogens, removal of debris such as apoptotic cells, myelin or excess synapses, and modulation of neuronal function and synaptic activity. They also secrete a wide array of pro- and anti-inflammatory chemokines and cytokines, ultimately shaping brain function and behavior [26, 32, 33, 46]. Microglia are highly dynamic and can adopt complex and diversified molecular, functional and morphological features when confronted with neuropathology [16, 22, 28, 44, 45, 47]. Neuropathological features adopted by microglia modify disease progression and severity. To understand how human microglia (hMG) contribute to the etiopathogenesis of neurological disorders, for instance Alzheimer's disease (AD), it is critical to use appropriate models to expose microglia to pathophysiological relevant conditions.

Microglia are extremely sensitive to external cues, and they adapt their morphology and transcriptome very rapidly to changing environmental conditions [18]. Studies of mouse microglia in the brain have been instrumental to understand the complex cell state changes that characterize their responses to amyloid plaque pathology [11, 22, 24, 38, 50]. However, the heterogeneity of human microglia is not well recapitulated in mouse microglia [17] hindering the translatability of these findings in AD mouse models to the human disease situation. One third of putative AD risk genes lack adequate mouse orthologs [29]. The transcriptional response of human microglia to AD pathology appears more elaborate, showing strong cytokine responses and antigen presentation reprogramming [28]. This emphasizes the importance of studying human cells to understand human disease [1, 6, 30]. Despite great strides in *in vitro* methods for studying hMG function [5, 13], *in vitro* hMG show a very different expression profile than primary human microglia, e.g. lacking expression of homeostatic markers (e.g. P2RY12, CSF1R, CX3CR1) while upregulating markers of activation (e.g. APOE, GPNMB) [29].

To overcome these issues, we and others have developed a xenotransplantation model, where hMG are xenografted into the mouse brain. Over time, those hMG colonize and tile the brain, adopt various morphologies depending on their activation status and show a transcriptional profile that is highly akin to primary hMG from human brain [28, 29]. This model has thus become an essential and powerful tool to study the behavior and function of human microglia [15, 20, 28, 29, 43, 49].

Successful transplantation entails a few challenges, including overcoming immune rejection and ensuring the provision of the correct growth factors to allow efficient and long-term engraftment of human microglia [1]. These requirements thus necessitate an optimal differentiation protocol to ensure the generation of the correct microglia precursor cells able to engraft the brain [15].

A key requisite is the inactivation of a functional adaptive immune response by T and B cells (achieved by a NOD SCID or *Rag2*^{-/-} genetic background) or innate NK cell activity (achieved through *Il2rg*^{-/-}, e.g., NOD SCID; *Il2rg*^{-/-} (NSG) or *Rag2*^{-/-}; *Il2rg*^{-/-}) [42]. Additionally, these models are engineered to express human cytokines (e.g. CSF1 alone or in combination with IL3, CSF2) and thrombopoietin (THPO) supporting the development and function of monocytes, macrophages and NK cells [1]. Hasselmann and Mancuso demonstrated that the expression of human IL3, CSF2 and THPO were not essential for survival and functional development of human microglia [20, 28, 29]. CSF1 signalling is essential for the survival and proliferation of xenografted microglia [1, 29]. Whereas murine CSF1 is not sufficient to support human microglia, the mouse CSF1 receptor responds equally well to hCSF1 as to mCSF1 and therefore expression of hCSF1 allows to support efficient differentiation and function of both human and murine myeloid cells [34]. Replacing mouse *Csf1* with human *CSF1* prevents the deleterious effects associated to CSF1 deficiency, including the deficits in bone and haematopoiesis [34, 51].

By genetically ablating the mouse microglia, full hMG chimerism can be achieved, but this requires the additional removal of the *Fms* intronic regulatory element (FIRE-enhancer) within the *Csf1R* locus of mouse genome. [2, 32, 36]. The generation of these host mice requires the combination of multiple transgenes, which makes it complex and expensive to generate those lines. Furthermore, patent restrictions (Regeneron patent EP2675271B1) on certain gene combinations (e.g. *Rag2*^{-/-}, *Il2rg*^{-/-}) found in the available *Rag2*^{tm1.1Flv}; *Csf1*^{tm1(CSF1)Flv}; *Il2rg*^{tm1.1Flv/l} mouse make that current models are not freely circulating among the researchers needing the models and hindering industry-academia collaborations for pre-clinical therapy development.

To overcome these issues and enhance future studies involving the xenotransplantation of hMG in mouse brain, we generated a new immune-deficient mouse model named *hCSF1*^{Bdes}, which combines *Rag2*^{-/-} and human *CSF1* knock in (KI) on a C57Bl6J background, the most widely used mouse strain for modelling human diseases through genetic modifications. This makes our model particularly attractive for crossbreeding with various human disease models, minimizing genetic

background variations that could otherwise influence experimental outcomes. We demonstrate here that the combination with *Il2rg*^{-/-} is dispensable for hMG xenotransplantation. We bred *hCSF1*^{Bdes} onto 2 widely available models used for AD research, *App*^{Hu} and *App*^{SAA} [40, 48] and show that xenografted hMG are able to mount the previously described amyloid response in these new mouse models [28].

Material and methods

Mice

hCSF1 knock in

CRISPR/Cas9 technology was used to replace the genomic DNA sequence corresponding to amino acid 33–552 of the mouse *Csf1* gene with the human *CSF1* genomic sequence corresponding to amino acid 33–554 in the endogenous gene. The 5' murine signal peptide (amino acid 1–32) and 3' region of the mouse were retained. The gRNA's (target sequence ACAGTGTTCTGACACCTCCTTGG and GTGGAAGTCCAGTATAGAAAGG) to the mouse *Csf1* gene, the donor vector (PCR assembled from BAC: RP23-15F10 (Mouse) and BAC: RP11-101M23 (Human)), and Cas9 mRNA were co-injected into fertilized mouse eggs of C57BL6J mice. F0 founder animals were identified by extensive PCR analysis followed by Sanger sequence analysis. F0 were bred to wildtype mice to test germline transmission and generate F1 animals. F1 animals were backcrossed to wildtype mice to generate F2 (Additional Fig. 1A). This line is called *Csf1*^{em1(CSF1)Bdes}.

Rag2 knock out

Crispr/Cas9 technology (target sequence AACATAGCC TTAATTCAACCAGG and ACGAGTCTGTAAACCG GCTACTGG and Cas9 enzyme) was used to generate an F0 founder in C57Bl6J mice. The F0 founder was selected by extensive analysis utilizing PCR and sequencing which demonstrated a 1198 bp genomic DNA deletion which corresponds to amino acid 16–430 and generates a premature stop (Additional Fig. 1B). The F0 founder was backcrossed two times to wildtype mice and the F2 generation was used to generate *Csf1*^{em1(CSF1)Bdes}; *Rag2*^{em1Bdes} mice, hereafter named *Csf1*^{Bdes}.

Standard genotyping is done by PCR with the following primers: *Csf1*^{Bdes} allele, AGAGTTAGACAGTTCTGG GTCTTT and ACTGGGTACCTGGAGATAGTT resulting in an amplicon of 252 bp, *Csf1*^{WT} allele, CCCTTG CCCTAAGGAGATAAA and ACTGGGTACCTGGAG ATAGTT resulting in a 355 bp amplicon, *Rag2*^{Bdes} allele, AGTGTCTGTGATTTCCCTAACGG and ACAATAGAT CATGGCGGGTTTA resulting in an amplicon of 320 bp, *Rag2*^{WT} allele GAGATGTCCCTGAACCCAGA and

TTGAGTGAGGATTGCACTGG resulting in an amplicon of 404 bp.

App knock in

The new xenograft model mouse was crossed with: (1) *App*^{em1Bdes} harbouring G676R, F681Y, R684H amino acid substitutions which humanize the A β sequence, previously extensively characterized and proposed here as control model [40]. We call this cross *App*^{Hu}. (2) With *App*^{tm1.1Dnli} (Jax strain 034711) harbouring G676R, F681Y, R684H amino acid substitutions to humanize the A β sequence and the KM670/671NL (Swedish), E693G (Arctic), and T714I (Austrian) amino acid substitutions which are well known FAD causing mutations [48]. These mice are called *App*^{SAA}. All the mouse lines and crosses are deposited with EMMA and free to use.

App^{tm3.1Tcs} [37] crossed with *Rag2*^{tm1.1Flv}; *Csf1*^{tm1(CSF1)Flv}; *Il2rg*^{tm1.1Flv/J}, (Jax strain 017708) named *App*^{NLGF}; *CSF1*^{Flv} and C57BL6JRj (Janvier labs), named WT, were used during the study in control experiments. Both male and female mice have been included in this study. Mice were analysed at the indicated time (see Figure legends). Mice had access to food and water ad libitum and were housed in an SOPF + facility with a 14/10-h light/dark cycle at 21 °C and 32% humidity, in groups of 2–5 animals. All experiments were conducted according to protocols approved by the local Ethical Committee of Laboratory Animals of KU Leuven (P125-2022).

Cell culture

Human embryonic stem cells (hESC; WA09 WiCell Research Institute, CVCL 9773) and human induced pluripotent stem cells (iPSCs; UKBi011-A-3, EBiSC) were differentiated into microglia progenitors according to the MIGRATE protocol [15]. After culturing the stem cells to 70–80% confluency, cells were detached and plated at 10 000 cells/well into a U-bottom 96-well plate. Cells were plated in mTeSR1 media (Stemcell Technologies, 85,850) supplemented with 50 ng/ml BMP4 (PeproTech, 125–05), 50 ng/ml VEGF (PeproTech, 100–20) and 20 ng/ml SCF (PeproTech 300–07) to induce embryonic body (EB) formation. On day 4 after plating, EBs were collected and transferred into a 6-well plate in X-VIVO 15 media supplemented with 50 ng/ml SCF (PeproTech 300–07), 50 ng/ml M-CSF (PeproTech, 300–25), 50 ng/ml IL-3 (PeproTech, 200–03), 50 ng/ml Flt3-ligand (PeproTech, 300–19) and 5 ng/ml TPO (PeproTech, 300–18). To induce myeloid lineage producing progenitors, EBs cell culture media was replaced with X-VIVO 15 media supplemented with 50 ng/ml Flt-3-ligand (PeproTech, 300–19), 50 ng/ml M-CSF (PeproTech, 300–25) and 25 ng/ml GM-CSF (PeproTech, 300–03) on day 11 of the protocol. On day

18 of the protocol, progenitors were harvested in PBS and transplanted into mouse brain. Throughout the protocol, cells were maintained in a humidified incubator at 37 °C and 5% CO₂.

Xenotransplantation of human microglia progenitors

To deplete endogenous mouse microglia, newborn mice were injected intraperitoneally with 200mg/kg body weight CSF1R inhibitor BLZ945 (Seleck, S7725) at the age of P2 and P3. At P4, mice were injected with microglia progenitors collected as described above on day 18 according to the MIGRATE protocol [15]. Mice were first anesthetized by hypothermia, after which they received bilateral injection (coordinates from bregma: anteroposterior, -1 mm, mediolateral, ±1 mm) of cell suspension containing progenitors (1 µl, 250 000 cells/µl). After recovering under an infrared lamp, pups were transferred back to their mothers.

Human microglia isolation

Mice were sacrificed by an overdose of sodium pentobarbital and subsequently perfused with ice-cold heparinized PBS. Brains were dissected into the left and right hemisphere, where one hemisphere was fixed in 4% PFA, and the other was processed for tissue homogenization, hMG isolation and assessing the presence of immune cells in the brain by FACS. Brain tissue was enzymatically dissociated using the Neuronal Dissociation Kit (P) (Miltenyi, 130-092-628) following manufacturer's instructions. After dissociation, tissue was passed through a 70µm cell strainer and pelleted for 15 min at 300 g at 4 °C. To remove myelin, pellets were resuspended in 30% Percoll solution and centrifuged for 15 min at 300 g at 4 °C, creating a myelin layer, which was carefully removed. The remaining cell pellet was washed with FACS buffer (2% FBS (Life Technologies, 10,270,106)), 2 mM EDTA (Sigma-Aldrich, E7889) in PBS) and blocked with FcR blocking solution (1:10, Miltenyi, 130-092-575 & 130-059-901) for 10 min at 4 °C. One-fourth of the sample was used for FACS analysis (see below) and the remainder was stained with viability dye eFluor780 (1:1000, Thermo Fisher, 65-0865-14) and antibodies for 30 min at 4 °C: anti-CD11b (1:50, Miltenyi, 130-113-806), anti-hCD45 (1:50, BD Bioscience, 555,485), anti-mCD45 (1:200, BD Bioscience, 563,890). Samples were run on the BD FACSCanto™ flow cytometer or Miltenyi MACS Quant Tyto cell sorter. After gating for CD11b⁺ cells, mouse microglia were defined as mCD45⁺ and hMG as hCD45⁺ cells. Data was analyzed using FlowJo software. Xenotransplanted hMG used for RNA sequencing were sorted on the Miltenyi MACS Quant Tyto cell sorter.

RNA isolation

Sorted hMG were lysed in 300 µl RLT buffer as supplied in the Qiagen RNeasy Kit and further processed for RNA isolation using the RNeasy Mini Kit (Qiagen 74,104) following manufacturer's instructions. Lysates were mixed with an equal volume of 70% ethanol and transferred to columns provided in the Kit. Columns were then washed sequentially with RW1 and RPE buffer provided in the Kit. As last step, RNA was eluted in 45 µl RNA-free water and stored at -80 °C.

FACS

Lymph nodes, spleens and brain were collected from mice sacrificed and perfused as above, in FACS Buffer. Single-cell suspensions from lymphoid organs were prepared by mechanical dissociation. Blood, spleens and lymph nodes were processed on a 70-µm pore-sized strainer in FACS Buffer, and cells were centrifuged for 5 min at 300 g. Red blood cell lysis was performed by using 1× red blood cell lysis buffer (420,301, Biolegend). Single-cell suspensions from brain tissue were prepared as described above.

Single cells were resuspended in FACS Buffer and incubated for 15 min on ice with FcR Blocking reagent (Miltenyi, 130-092-575). Surface staining was performed for 45 min on ice using the following antibodies; anti-CD45 (Clone 30-F11, Biolegend), anti-CD3(145-2C11, Biolegend), anti-CD19 (Clone 1D3, Biolegend), anti-NK1.1 (Clone PK136, Biolegend), anti-MHCII (Clone M5114.15.2, Biolegend), anti-CD11b (Clone M1/70, BD bioscience). Death cells have been excluded from the analysis using the eBioscience Fixable Viability Dye eFluor780 (1:1000, Thermo Fisher, 65-0865-14). Cells were washed and resuspended in FACS buffer before flow cytometric analysis on a Fortessa X-20, using the FACS-Diva software. Data were analyzed using FlowJo (TreeStar, Version 10.7).

Immunohistochemistry and microscopy

The same mice were used for immunohistochemistry and bulk RNA sequencing at 6 months of age. The 4% PFA post-fixed brain hemispheres of both *App^{Hu}* (2× females, 3× males) and *App^{SAA}* (3× females, 2× males) mice were sectioned coronally on a vibratome (30µm). Sections used for Aβ staining, underwent antigen retrieval using 10mM Sodium Citrate buffer pH 6.0 (VWR). Sections were washed 3×5min in phosphate-buffered saline (PBS), followed by 15min permeabilization using PBS with 0.2% Triton X-100 (PBST) and a 20min incubation at room temperature (RT) with X34 staining solution [10 µM X34 (SML1954-5MG, Sigma-Aldrich) diluted in 60% PBS (vol/vol), 40% ethanol (vol/vol) and 20mM NaOH

(Sigma-Aldrich)]. Following 3×2min washes using 60% PBS (vol/vol) with 40% ethanol (vol/vol), and 2×5min PBST washes, followed by blocking and permeabilization of all sections in blocking buffer (5% donkey serum in PBST) for 1h at RT. After overnight incubation with the primary antibodies [1/200 anti-HLA DR+DP+DQ clone CR3/43 (ab7856 Abcam), 1/1000 anti-P2RY12 (HPA014518 Atlas Antibodies), 1/200 82E1 (10,323 IBL-America), 1/500 anti-ibal (234,004 Synaptic Systems), 1/200 anti-Nuclei (MAB1281 Milipore)] in blocking buffer at 4°C, sections were washed 3×5min in PBS. Next, sections were incubated for 2h at RT in secondary antibodies in blocking buffer [donkey anti-rabbit Alexa488 (A21206, Invitrogen), donkey anti-mouse Alexa594 (A21203, Invitrogen), donkey anti-guinea pig Cy5 (706–175-148, Jackson ImmunoResearch Inc.), donkey anti-mouse Alexa647 (A31571, Invitrogen), goat anti-guinea pig Alexa488 (A11073, Invitrogen), donkey anti-rabbit Alexa555 (A31572, Fisher Invitrogen) all 1/500] and washed 3×5min in PBS. Sections for the A β and hMG staining were mounted in Glycergel (C056330-2, Agilent) or FluorSave (345,789, Millipore). Sections for the HLA/CD9 staining were again blocked for 1h in blocking buffer, followed by an overnight incubation with the second set of primary antibodies [1/100 anti-CD9-biotin (312,112, Biolegend) and anti-P2RY12]. The next day, sections were washed 3×5min in PBS and incubated for 2h at RT with the secondary antibodies [1/500 donkey anti-rabbit Alexa594 (A21207, Invitrogen) and 1/500 Streptavidin Alexa488 (S32354, Thermo Scientific)], again washed 3×5min in PBS and mounted using Glycergel. Slides were kept at 4°C until imaging. Confocal images were acquired using a Nikon AX inverted microscope driven by NIS (v5.42.06) software. For excitation, 405nm, 488nm, 561nm and 640nm laser lines were used. Images were acquired using a 4x (NA=) or 20x (NA=) objective lens and processed using Fiji/ImageJ software. Images shown in Fig. 2 were acquired using a Nikon Eclipse slide scanner. Images were acquired using a 10× objective lens and processed using QuPath software.

Western blot analysis

Fifty micrograms of cleared protein brain lysate (in 250 mM sucrose, 1 mM EGTA, 5 mM Tris–HCl pH 7.4) supplemented with 1% TX-100 and cOmplete protease inhibitor cocktail (Roche) was loaded in reducing and denaturing conditions on NuPAGE (Thermo Fisher Scientific) gels and subjected to electrophoresis. Following separation, proteins were transferred to a nitrocellulose membrane for Western blotting. Membranes were stained with Ponceau-S, imaged and blocked with 5% non-fat milk Tris-buffered saline, containing 0.1% Tween 20, and incubated with Anti-M-CSF antibody

[EPR20948] (Abcam) recognizing both human and mouse CSF1, washed, and incubated with horseradish peroxidase–conjugated secondary antibodies (Bio-Rad). Blots were developed using the ECL Renaissance kit (PerkinElmer) using a LAS-3000 Imaging System From Fuji.

CSF1 ELISA

Blood samples were collected in EDTA coated tubes and after clearing, plasma was subjected to ELISA using commercially available human CSF-1 (Thermo Fisher Scientific, EHCSF1) and mouse CSF-1 (Peprotech, 900-K245) ELISA kits according to the manufacturer's instructions.

Bulk sequencing

The same *App^{Hu}* (2×females, 3×males) and *App^{SAA}* (3×females, 2×males) mice were used for immunohistochemistry and bulk RNA sequencing at 6 months of age. RNA concentration and purity were determined spectrophotometrically using the Nanodrop ND-8000 (Nanodrop Technologies, Wilmington, DE, USA) and RNA integrity was assessed using a Bioanalyzer 2100 (Agilent Technologies, Inc. Santa Clara, CA, USA). Per sample, an amount of 1 ng of total RNA was used as input for the SMART-Seq HT PLUS protocol to generate full-length cDNA (version “011921”; Takara Bio USA, Inc) using a one-step RT-PCR, combining the reverse transcription and cDNA amplification into 1 step. Subsequently, 4 ng of purified double-stranded cDNA was enzymatically fragmented and stem-loop adapters were ligated. Libraries were then amplified and indexed, generating Illumina-compatible libraries with unique dual indexes (UDIs) according to the manufacturer's protocol [4].

Sequence-libraries of each sample were finally equimolarly pooled and sequenced on AVITI 2×75 Cloudbreak High, single read (101–8–8–0) at the VIB Nucleomics Core (www.nucleomics.be). Reads were aligned against a combined *mus musculus* (mm10) and *homo sapiens* (GRCh38) database using STAR (v.2.7.11a, [12], quality checked using FastQC (v.0.11.9, (Bittencourt SA, 2010)) and counted using featureCounts (v.2.0.1, [27]). MRNAs with fewer than 10 counts in at least 5 samples were discarded, leaving 15,504 human mRNAs for differential expression (DE) analysis using DESeq2 (v.1.42.1) in R (v.4.3.2.). To adjust for multiple testing, Benjamini–Hochberg *p*-value adjustment was performed.

Enrichment analysis

Gene Ontology enrichment analysis was performed using DAVID [21]. Enrichment for top marker gene sets for HLA (*n*=91 genes), DAM (*n*=89) and CRM (*n*=91) as published [28] was performed manually using the Chi-square test, testing for the overlap between the

different datasets and the genes significantly differentially expressed after p -value adjustment ($n=214$ total, overlap with DAM ($n=17$), HLA ($n=12$) and CRM ($n=13$)), while controlling for the total observed genes in the dataset ($n=15,504$). P -value adjustment on the chi-square obtained p -values was performed using Bonferroni.

Statistical analysis

Exemplar histological images and flow cytometry plots were selected to closely resemble expression patterns seen overall in the experimental group. Comparisons between two groups were performed using unpaired Mann Whitney U tests, for 3 groups 1-way or Welch's ANOVA was used. The value of n reported within Figure legends represents the number of animals, unless otherwise specified. Values are represented as the mean \pm SD, with differences considered significant when $p < 0.05$. Graphs were prepared with GraphPad Prism (GraphPad Software v9.5.1) or R (v.4.3.2).

Results

Generation of the mice

The successful engraftment of human microglia depends on the expression of humanized CSF1 as human CSF1R signalling cannot be fully activated by murine CSF1. To avoid rejection, depletion of T and B cells is also necessary [41]. We used CRISPR/Cas9 to interchange the part of mouse *Csf1* gene encoding amino acids 33–552 with the human counterpart corresponding to amino acids 33–554. Regulatory elements such as the promoter, 5'UTR, murine signal peptide (amino acid 1–32) and 3'UTR of the mouse were preserved by this targeting (Additional Fig. 1A). The *Rag2* gene was targeted by a CRISPR/Cas9 strategy resulting in the deletion of amino acids 16–430 and the introduction of a premature stop codon (Additional Fig. 1B). Founder mice were generated in the C57Bl6J background and backcrossed over two generations to cross out potential unwanted off target events from the gene editing. Then they were intercrossed to generate the new immune deficient mouse model that we named *hCSF1^{Bdes}*. The mouse was crossed

with *App^{Hu}* and *App^{SAA}* mice [40, 48]. While CRISPR/Cas9 technology to generate this model is patented, most academic institutions have the required permissions that enable the use of this model. Commercial entities must ensure they have the appropriate licenses for CRISPR/Cas9 technology generated materials.

Physiological expression levels of human CSF1 in the knock-in model

The new *hCSF1^{Bdes}* mice are fertile, healthy, produce normal litter size and show no obvious abnormal behaviour. As physiological expression levels of CSF1 are of major importance for health [19, 25] we evaluated the expression levels of human CSF1 in brain and blood from the humanized *hCSF1^{Bdes}* KI mice and compared those levels with WT mice. Brain CSF1 levels analysed by western blot (Fig. 1A) are comparable between the two strains. Next, we measured the levels of CSF1 in the blood from WT, homozygous and heterozygous *hCSF1^{Bdes}* mice by ELISA (Fig. 1B). As expected, WT mice expressed only mouse CSF1, *hCSF1^{Bdes}* heterozygous mice expressed both mouse and human CSF1 and homozygous *hCSF1^{Bdes}* mice expressed only human CSF1. For the measurements we used kits from two different companies with their own calibrators, which makes a direct comparison of absolute values between the measurements relative, yet values are within the reported range. Summarized, we demonstrated normal physiological expression of human CSF1, i.e. not exceeding the levels of mouse CSF1, in brain and blood.

The novel *hCSF1^{Bdes}* mice lack mature lymphocytes

The *hCSF1^{Bdes}* mice lack the *Rag2* gene, whose gene product is an essential component of the V(D)J recombinase system which results in the absence of mature B cells and T cells. Consequently, the weights of the spleen and thymus were significantly lower in the *hCSF1^{Bdes}* mice than in WT mice, while body weight was unaffected (Fig. 1C) resembling other *Rag2* KO strains [35, 41] (Additional Fig. 2). The presence of live, CD45^{high} lymphoid cells was analyzed in the spleen (Fig. 1C), and in lymph nodes

(See figure on next page.)

Fig. 1 Characterization of CSF1 expression and *Rag2*^{-/-} effects in *hCSF1^{Bdes}* mice **A**. CSF1 expression in brain of homozygous *hCSF1^{Bdes}* and WT (C57BL/6J) mice (mixed sexes, 11 weeks of age) was assessed by western blot analysis with an antibody recognizing both human and rodent CSF1 (left panel), showing equal expression levels. The right panel represent the Ponceau S staining as loading control. Position of molecular weight markers are indicated. **B**. CSF1 expression in the plasma from homozygous and heterozygous *hCSF1^{Bdes}* and WT mice measured with ELISA. mean, SD and $n=2-6$ are presented on the graph. **C**. Spleen, thymus and body weight in *hCSF1^{Bdes}* mice compared to Wild type (WT; C57BL/6j) mice by Mann Whitney U test. Bar plots represent mean \pm SD, $n=6-7$. **D-F**. FACS analysis of lymphocytes and NK cells in *hCSF1^{Bdes}* mice (mixed sexes, 11 weeks of age). Single cells were isolated from the spleen and lymph nodes and stained with anti-CD3, anti-CD19, anti-NK1.1, anti-CD45 and anti-CD11b antibodies, and analyzed by flow cytometry. (D) Representative gating strategies to identify T-, B-, NKT cells and NK cells in spleen (left) and Lymph nodes (right) in WT mice. The histograms represent (E) the distribution and total count of lymphoid cells in spleen, and (F) their distribution in lymph nodes. $n=4-5$, bar plots represent mean \pm SD. *hCSF1^{Bdes}* mice are compared to the WT mice by Mann Whitney U test

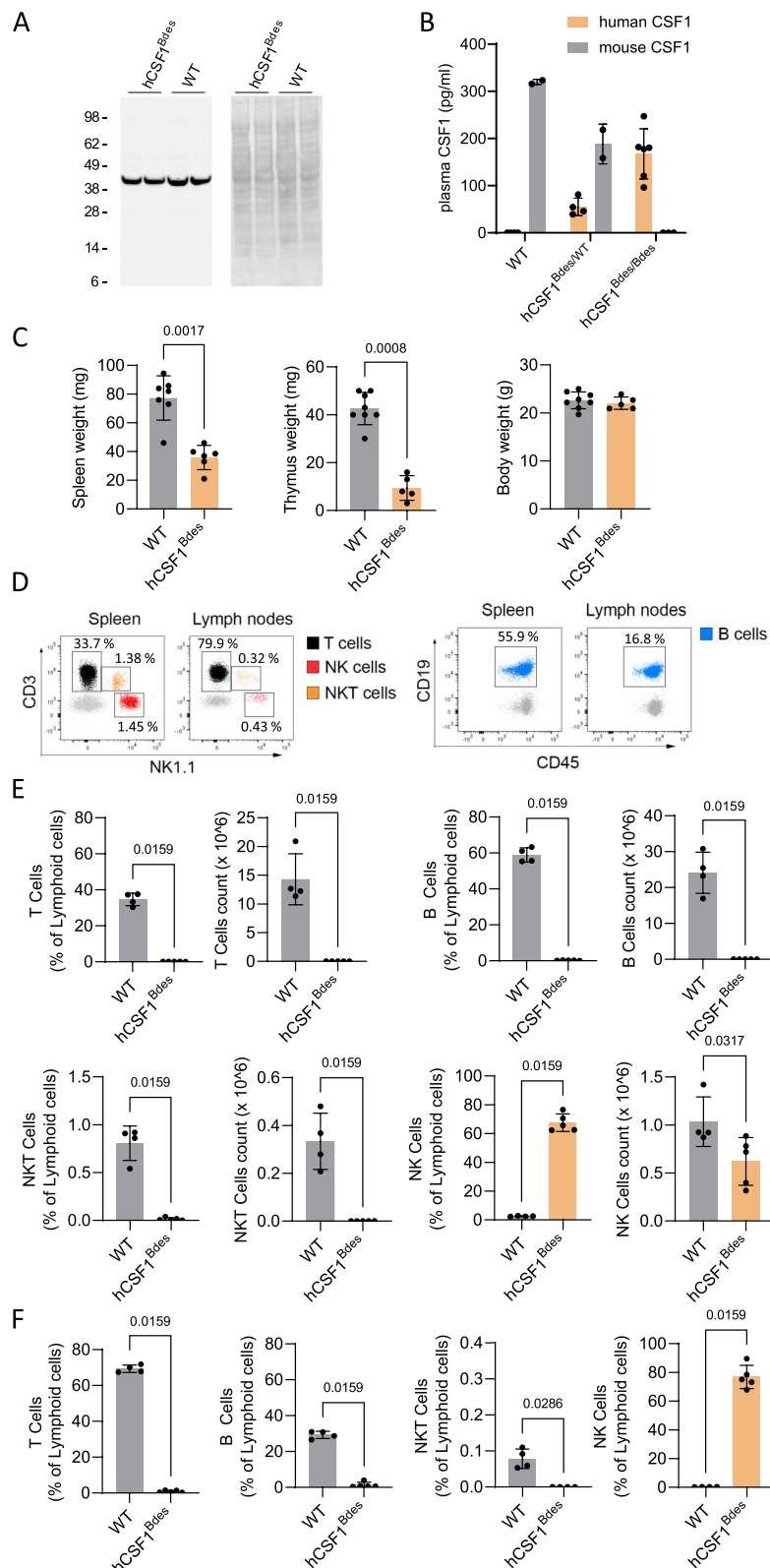


Fig. 1 (See legend on previous page.)

(Fig. 1D) using flow cytometry. Expression of specific markers allowed identification of different subsets such as T cells (CD3⁺, NK1.1⁻, CD19⁻), natural killer (NK) T cells (CD3⁺, NK1.1⁺, CD19⁻), NK cells (CD3⁻, NK1.1⁺, CD19⁻) and B cells (CD3⁻, NK1.1⁻, CD19⁺). As expected *hCSF1^{Bdes}* mice lack T cells, B cells and NK T cells in lymphoid organs. Innate immune cells are, however, present in the *hCSF1^{Bdes}* mice, including NK cells. The percentage of NK cells in spleen and lymph nodes appears increased in *hCSF1^{Bdes}*. The increase in percentage is due to the lack of mature B and T cells: i.e. the immune niche of lymphoid tissues is empty and therefore this higher percentage does not reflect an actual increase in the NK population. When considering cell counts, we observed a slight reduction in NK cell number, which is expected due to the reduced size of the spleen in these immune deficient mice (Fig. 1D-F). Importantly, the number of NK cells in the brain of both WT and *hCSF1^{Bdes}* is neglectable with maximally 0.005% NK cells in the single cell brain suspension (Additional Fig. 3). There is no increase in the NK population, as demonstrated by measuring the absolute count of NK in the spleen (Fig. 1E).

In summary, we confirmed that the *hCSF1^{Bdes}* mouse model recapitulates immunological features linked to RAG2 deficiency [35, 41].

Efficient xenotransplantation of human microglia in the model

Utilizing our previously published protocol [15] we transplanted hMG progenitors derived from the embryonic stem cell line H9 (WAE009-A, Wi-Cell) in *hCSF1^{Bdes}* mice at postnatal day P4. One- and 3-months post-transplantation the percentage of hMG was estimated by flow cytometry. One month after the transplantation the percentage of hMG, defined as hCD45⁺ cells, out of the total microglia number (hCD45⁺ and mCD45⁺) was around 50% (Fig. 2A-C), implying half of the microglia in the mouse brain were of human origin. At three months after xenotransplantation the number of hMG reached levels up to 68% of the total pool of microglia (Fig. 2B-C). Using the same protocol, we also tested hMG derived from an induced pluripotent stem cell (iPSC), namely UKBi011-A-3, and xenotransplanted them into *hCSF1^{Bdes}*. Similarly to H9-derived microglia, we observed around 50% hMG in the brains of engrafted mice 1- and 6-months post-transplantation (Additional Fig. 2), which resembles graft efficiencies in *hCSF1^{Flv}* mice [15, 28].

We further investigated the spread and morphology of transplanted hMG by immunohistochemistry. Microglial cells, both mouse and human, were stained using the well-established Iba1 marker. hMG were further distinguished using the human-specific P2RY12 antibody, and a human nuclei (hNu) staining. We observed widespread

distribution of hMG, defined as P2RY12⁺ and hNu⁺ cells, in the mouse brain 3 months after transplantation (Fig. 2D). Furthermore, engrafted hMG showed their typical ramified microglial morphology (Fig. 2D) as described before [20, 29].

In summary, we confirm that human stem-cell derived microglial progenitors can be successfully xenotransplanted into the brains of *hCSF1^{Bdes}* mice. After the xenotransplantation, hMG progenitors acquire their typical ramified morphology and colonize the mouse brain efficiently.

The new model enables to study the hMG response to Alzheimer's amyloid-β pathology

We next assessed the utility of the *hCSF1^{Bdes}* mouse for researching the hMG response to amyloid-β pathology by crossing it to the freely available *App^{SAA}* mouse [48] as well as a control mouse that carries the humanized amyloid-β sequence without any pathological mutations (referred to as the *App^{Hu}* mice [40]). Both mouse strains were xenotransplanted with H9-derived hMG at P4 and graft efficiency in both mouse strains was assessed at 6 months post xenotransplantation, showing similar graft efficiencies for both strains (see Fig. 3A-B). Additionally, staining the mouse brain for hMG using the hMG marker hP2RY12 showed widespread distribution of hMG in 6-month-old *App^{Hu}* and *App^{SAA}* mice, with hMG inhabiting areas with amyloid plaque deposits in *App^{SAA}* mice (Fig. 3C) as defined by 82E1⁺ and/or X34⁺ areas.

Next, we wanted to assess whether xenotransplantation per se, or the creation of a pro-inflammatory milieu in the presence of Aβ pathology, would facilitate an influx of NK cells into the brain. Using FACS, we could not find differences in the number of NK cells in the brain of WT, *App^{Hu}* or *App^{SAA}* mice (Fig. 3D), nor could we observe differences in the number of NK cells in their blood (Fig. 3E).

To estimate the effect of NK cell presence on grafting efficiency of human microglia, we assessed the percentage of hMG in the brains of *App^{SAA}* and *App^{NLGF};CSF1^{Flv}* mice xenotransplanted with the same batch of H9-derived hMG (Fig. 3F). We show here no differences in the percentage of hMG in mice with (*App^{SAA}*) and without NK cells (*App^{NLGF};CSF1^{Flv}*) in the brain (Fig. 3F).

At 6 months of age, the response of hMG to amyloid pathology was assessed by bulk RNA sequencing on sorted hMG and immunohistochemistry. Differential expression analysis comparing the transcriptome of sorted hMG xenotransplanted in the *App^{Hu}* vs the *App^{SAA}* mice revealed 214 significantly differentially expressed genes (padj < 0.05), with 152 upregulated and 62 downregulated genes. Among the top upregulated genes were

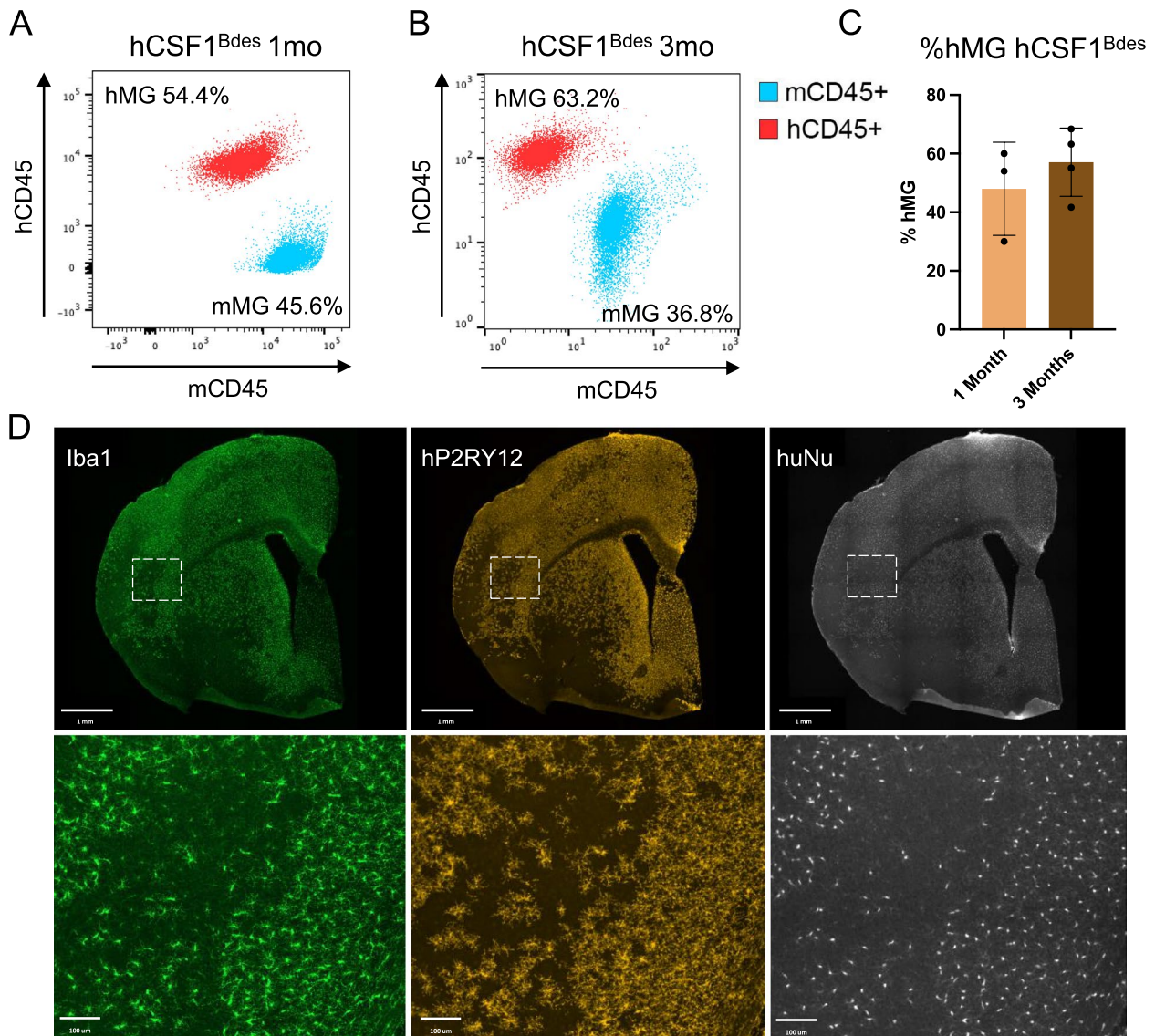


Fig. 2 Efficient xenotransplantation of human derived microglia. **A-C.** Representative flow plots (**A-B**) and quantification of hMG % (**C**) for *hCSF1^{Bdes}* mice xenografted with human microglia, 1 month (**A**) and 3 months (**B**) after xenotransplantation. Human microglia (hMG) are represented as *hCD45⁺* population after gating for *CD11b⁺* cells. Mouse microglia (mMG) are represented as *mCD45⁺* population after gating for *CD11b⁺* cells. Samples were acquired on BD FACSCanto flow cytometer (**A**) or Miltenyi Quant Tyto cell sorter (**B**) and analysed in FlowJo software (**C**). *n* = 3–4, bar plot represents mean ± SD. **D.** Representative images of engrafted human microglia in the brain of *hCSF1^{Bdes}* mice at 3 months of age. Microglia cells (both mouse and human) are identified as *Iba1⁺* cells. Xenografted human microglia are identified as *hP2RY12* and *hNu* positive cells. Scalebar, 1mm (top) and 100µm (bottom)

CD83, *RGS16* and *CD9* whereas *CLDN4*, *TMEM176B* and *SOX5* were most downregulated (Fig. 4A).

Our lab has demonstrated previously that the hMG response to Aβ pathology is more complex and multifaceted than the mouse response [28]. By using the top marker genes for disease-associated microglia (DAM), antigen presenting microglia (HLA) and cytokine response microglia (CRM) from Mancuso et al. [28] we could demonstrate a significant enrichment of DAM

(Chi-square (1, *n* = 15,504) = 147.6, *p*adj = 6.6e-16), HLA (Chi-square (1, *n* = 15,504) = 69.8, *p*adj = 6.6e-16) and CRM genes (Chi-square (1, *n* = 15,504) = 82.9, *p*adj = 6.6e-16) among the DE genes, demonstrating the ability of hMG within the *App^{SAA}* mice to mount a transcriptional response to amyloidosis that is similar to what we described previously in the *App^{NLGF}* mice (Fig. 4B). GO enrichment analysis using DAVID (Fig. 4C) further confirms that hMG within the *App^{SAA}* mice deregulate

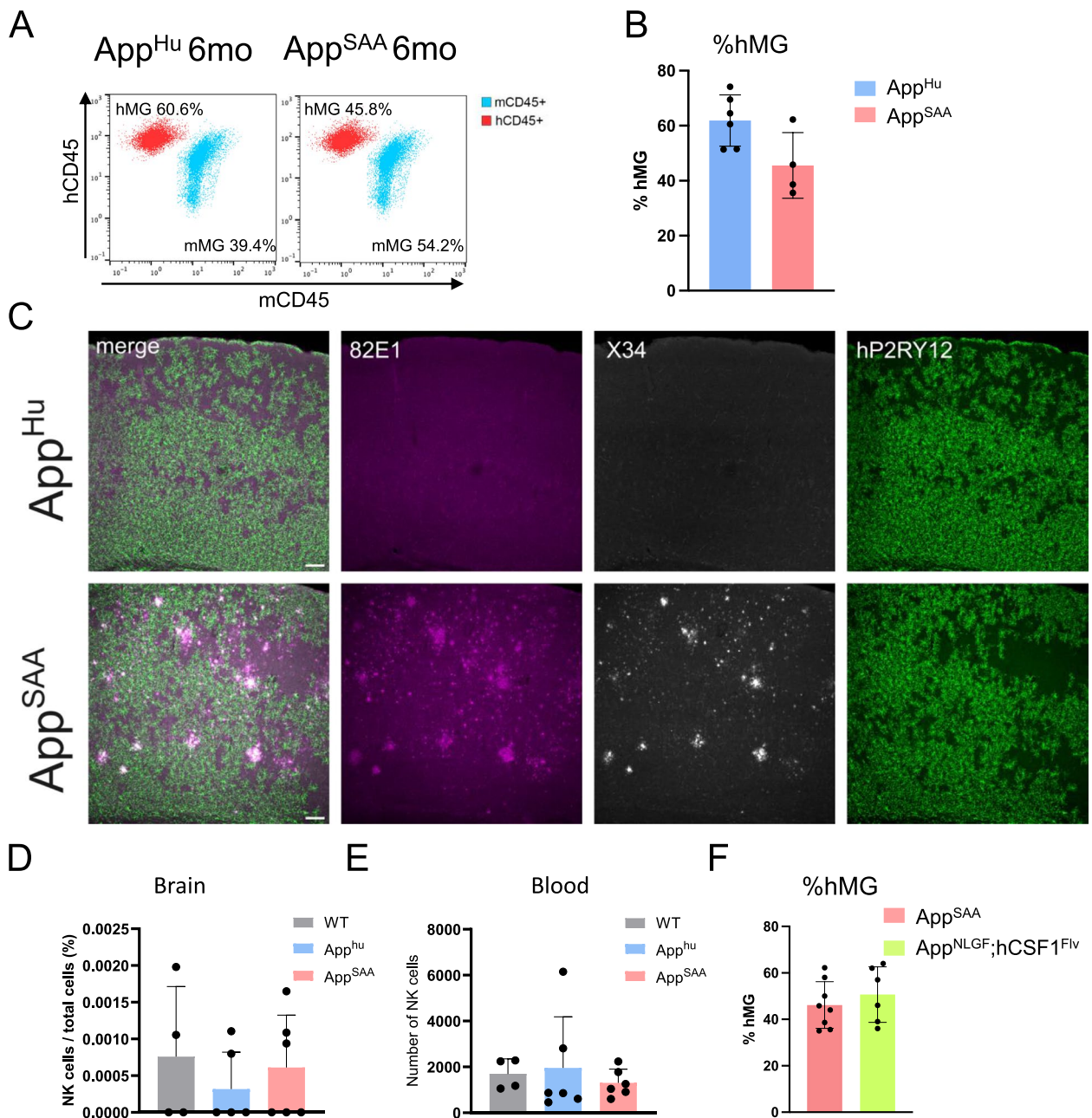


Fig. 3 Human microglial response to A β pathology. **A-B.** Representative flow plots (**A**) and quantification of hMG % (**B**) for xenografted *App^{Hu}* (panel A left) and *App^{SAA}* (panel A, right) mice 6 months after xenotransplantation. Human microglia (hMG) are represented as hCD45⁺ population after gating for CD11b⁺ cells. Mouse microglia (mMG) are represented as mCD45^{mid} cells after gating for CD11b⁺ cells. Samples were acquired on BD FACS Canto flow cytometer (**A**) or Miltenyi Quant Tyto cell sorter (**B**) and analysed in FlowJo software $n=4-6$, bar plot represents mean \pm SD. **C.** Representative images of human microglia engrafted in the cortex of *App^{Hu}* and *App^{SAA}* mice at 6 months of age, labeled with human-specific antibodies for hP2RY12, as well as X34 and 82E1 for A β plaques. Scale bar, 100 μ m. **D-E.** Single cells have been isolated from mouse brain (half brain hemisphere) (**D**) and 100 μ l of blood (**E**) and analysed by FACS. The graph represents FACS quantification of NK cell number in 6 months old *App^{Hu}* and *App^{SAA}* xenografted with hMG and in WT mice (C57BL6Jrj, not grafted). Bar plot represents mean \pm SD ($n=4-6$, one-way ANOVA (D), Welch's ANOVA (E)). **F.** FACS quantification of % hMG in 6-7-month-old xenografted *App^{SAA}* and *App^{NLGF};hCSF1^{Flv}* mice. $n=6-8$, bar plot represents mean \pm SD, Mann Whitney U test

genes associated with the MHC-II response, clathrin-mediated endocytosis, phagosome and lysosome, which is in line with previously reported differentially expressed genes in hMG when facing amyloid pathology [10, 28]. By using immunohistochemistry we again confirm similar graft efficiencies between the strains (Fig. 4D) and find that 6 months old *App*^{SAA} mice display robust plaque pathology in regions xenotransplanted with hMG. We found that whereas expression of MHC-II genes was mainly restricted to the CNS-associated macrophages lining the bloodvessels and dura in *App*^{Hu} mice (white arrows Fig. 4E), as in accordance with literature [14, 39], *App*^{SAA} mice also display an upregulation of MHC-II as well as CD9 protein in the brain parenchyma and particularly in close vicinity to plaques (white arrow heads Fig. 4E left panel & zoom Fig. 4F). These observations are in line with our bulk RNAseq data and previous reports using other models of amyloidosis [9, 10, 20, 28]. In conclusion, these results demonstrate that the new *hCSF1*^{Bdes} mouse provides a valuable alternative for xenotransplantation experiments and studying the response of hMG to AD-relevant pathologies.

Discussion

Microglia xenotransplantation can be performed with success in the *hCSF1*^{Flv} mice (*Rag2*^{tm1.1Flv}; *Csf1*^{tm1(CSF1)^{Flv};Il2rg^{tm1.1Flv/J}}) [20, 29]. Humanization of CSF1 is required for the integration, survival and proliferation of human myeloid cells in the mouse environment [1, 15, 20, 28, 29, 43, 49]. Conversely, deletion of both *Rag2* and *Il2rg* genes ensures the absence of functional T cells, B cells and NK cells, which makes the *Rag2*^{tm1.1Flv}; *Il2rg*^{tm1.1Flv/J} the elective model for xenotransplantation. The *hCSF1*^{Bdes} mouse model that we generated expresses the *hCSF1* and lacks the *Rag2* gene, and therefore it lacks functional T cells and B cells, while NK are present in normal numbers (Fig. 1). In contrast to T and B cells, NK cells represent the innate lineage of lymphocytes that possess germline-encoded antigen receptors and they do not require RAG proteins for their development, function, or survival [23, 41]. Early activation of NK cells following transplantation is associated with killing of allogeneic target cells and release of immunomodulatory chemokines

and cytokines, which can contribute to rejection. However, there is no evidence that *Il2rg* deficiency is needed for human cell transplantation in brain [3].

We demonstrate here that we can successfully transplant iPSC-derived hMG into the brain of *hCSF1*^{Bdes} mice (Fig. 2), without eliciting an NK driven immune response. In general, the number of NK cells found in the brain is negligible, even after xenotransplantation (Additional Fig. 3, Fig. 3D). hMG could survive and were able to stably colonize a large area of the mouse brain (>50% of all microglia were human), and showed the typical ramified morphology and expression of homeostatic markers comparable to similar experiments performed in the *hCSF1*^{Flv} mice [28, 29, 49]. We further show that by crossing the *hCSF1*^{Bdes} mouse to the *App*^{SAA} mouse model of AD and *App*^{Hu} control mice, the xenografted hMG exposed to amyloid- β pathology in *App*^{SAA} upregulate the typical activation markers previously described, including CD9 and HLA-DQ/DR both on mRNA and protein levels, predominantly in the vicinity to plaques. Our data largely agree with our previous work confirming that the described phenotypes of the multipronged amyloid plaque response are maintained in this independent novel mouse model for studying human microglia responses in disease [28].

Thus, our *hCsf1*^{Bdes} mouse proves to be a valuable new alternative for the broader research community. Whereas the current standard in the field, the *hCSF1*^{Flv} is restricted to non-profit entities as dictated by the Regeneron patent EP2675271B1, our model demonstrates that the combination with *Il2rg*^{tm1.1Flv/J} is not needed for microglia transplantation. We furthermore humanized the *Csf1* locus and generated an entirely novel *Rag2* targeted allele. Users should take into account that RISPR/Cas9 technology was used to generate this novel model, and investigators need to check whether their institute is subject to the terms and conditions of the limited license from the Broad institute and from Caribou Biosciences, Inc. Thus, in principle, the *hCsf1*^{Bdes} mouse can be used by non-profit and for-profit organisations, facilitating the use of the xenotransplantation paradigm for hMG to study complex human disease. We also anticipate that this will further enable the exploration of the use of hMG

(See figure on next page.)

Fig. 4 Bulk RNAseq demonstrates the activation of hMG in response to A β pathology. **A.** Vulcano plot of the most differentially up- (red) and down-regulated (blue) genes (Benjamini–Hochberg corrected *p*-value (*padj*) < 0.05) when comparing the bulk RNAseq profile of sorted hMG engrafted in *App*^{SAA} (*n* = 5) vs *App*^{Hu} (*n* = 5) mice at 6 months of age. **B.** Vulcano plots highlighting the top 100 marker genes that were significantly differentially expressed (*padj* < 0.05) in this dataset for disease-associated microglia (DAM), antigen presenting microglia (HLA) and cytokine response microglia (CRM1) and as found in [28]. **C.** Significantly enriched gene ontology (GO) categories, Uniprot Keywords (UP-KW) and KEGG pathways as found by DAVID. **D–F.** Immunohistochemistry for hP2RY12 (**D**), hCD9, hHLA (HLA-DR/DP/DQ) and X34 (**E–F**) in 6 months old *App*^{SAA} vs *App*^{Hu} mice. **D–E,** scalebar visible in merge: 200 μ m. **E.** arrow-heads (left panel) pinpoint parenchymal plaque-associated hHLA and hCD9 staining in *App*^{SAA} mice, whereas arrows indicate hHLA staining in CNS-associated macrophages. **F.** Zoom of insert in merge from panel E, scale bar: 50 μ m

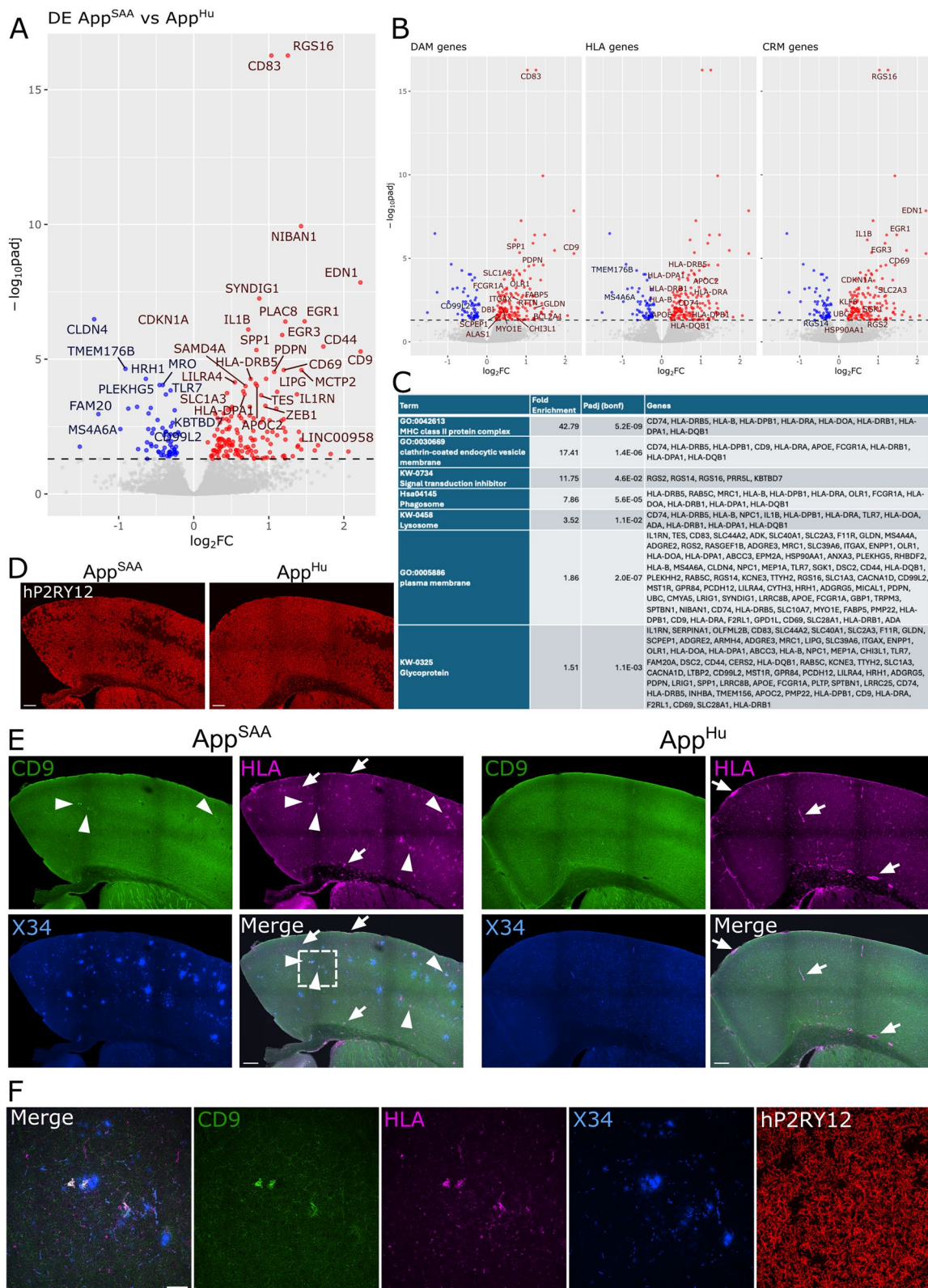


Fig. 4 (See legend on previous page.)

transplantation as a therapeutic modality for various diseases [7, 32] Particularly in combination with the newly developed CSF1R inhibitor-resistant human CSF1R variant [8]) and the broader advances the scientific community is making on the use of transplantation models for the treatment of neurological disorders such as epilepsy or Parkinson disease (Svendsen 2024 Nat Med), stem cell-based therapies using microglia may hold a place in disease treatment in the not-too distant future.

Conclusion

Our *hCSF1^{Bdes}* model demonstrates that NK cell depletion is not required for successful human microglia transplantation and further work validated the multipronged response of human microglia to amyloid plaques. This versatile new model is accessible to both non-profit and for-profit organizations, facilitating the broader application of the xenotransplantation paradigm with hMG to advance research on complex human diseases.

Abbreviations

AD	Alzheimer disease
CSF1	Colony stimulating factor 1
hMG	Human Microglia
IL2RG	Interleukin 2 Receptor Subunit Gamma
NK	Natural killer
RAG	Recombination activating gene
SD	Standard deviation

Supplementary Information

The online version contains supplementary material available at <https://doi.org/10.1186/s13024-025-00823-2>.

Additional file 1. Generation of the humanized *Csf1* and *Rag2* knock mice. A. Schematic overview of the strategy used to generate the humanized *Csf1KI* allele. Exons are presented as boxes; the positions of the guide RNA's are indicated. Primers used for quality control by PCR and Sanger sequencing are depicted as arrows. The mouse exons and introns presented in brown are replaced by human exons and introns indicated in green. The lower panel shows the Sanger sequencing results at the recombination sites. Genotyping primers are indicated with brown arrows (1) for the *Csf1^{WT}* allele and green (2) for the *Csf1^{Bdes}* allele. B. Schematic overview of the strategy used to generate the *Rag2^{Bdes}* KO allele. Exon3 of the mouse *Rag2* gene is depicted as a box, the complete open reading frame of the *Rag2* gene as a black box, the position of the two guide RNA's are indicated. The lower part shows the Sanger sequencing results at the deletion site demonstrating that 1198 bp of the coding sequence are deleted. The primers used to genotype the alleles are indicated with arrows, black arrows (3) for *Rag2^{WT}* allele and blue arrows (4) for *Rag2^{Bdes}* allele.

Additional file 2. Efficient xenotransplantation of human derived microglia in the *hCSF1^{Bdes}* mouse model. A-B. *hCSF1^{Bdes}* mice were xenografted with human microglia derived from iPSCs (UKBi011-A-3). Isolated microglia were analyzed by flow cytometry one month (A) and 6 months (B) after xenotransplantation. Human microglia (hMG) and mouse microglia (mMG) are represented as percentage of total CD11b⁺ cells. C. Graft efficiency of hMG at 1 and 6 months after transplantation. *n* = 2, bar plot represents mean ± SD.

Additional file 3. Single cells have been isolated from one hemisphere of a mouse brain and analysed by FACS. The graph represents FACS quantification of NK cell number in *hCSF1^{Bdes}* and in WT mice. We express the number of NK cells, as % of cells of the total isolated mouse cells. The

total number of cells we obtain from one mouse is variable, averaging ± 500.000 cells/mouse hemibrain (omitting cerebellum). Bar plot represents mean ± SD (*n* = 4, Mann Whitney U test).

Acknowledgements

The authors thank Amber Claes and Veronique Hendricks for breeding and taking care of the mice. The VIB-KU Leuven Center for Brain & Disease Research Technologies, Mouse Expertise Unit for rederivation of the mouse colonies and Daan Moechars for his help with the GEO submission. This work was funded by a FBRI research funding awarded to B.D.S. entitled "Generation and initial characterization of a humanized CSF1 Knock in model to study microglia function and dysfunction". This project received further funding from the European Research Council (ERC) under the European Union's Horizon 2020 Research and Innovation Programme (grant agreement no. ERC-834682 CELLPHASE_AD). This work was also supported by funding from UKRI and the Medical Research Council (MR/Y014847/1) via the Dementia Research Institute. Further support was given by the Flanders Institute for Biotechnology (VIB vzw), a Methusalem grant from KU Leuven and the Flemish Government, the Fonds voor Wetenschappelijk Onderzoek, KU Leuven, The Queen Elisabeth Medical Foundation for Neurosciences, the Opening the Future campaign of the Leuven Universitair Fonds, The Belgian Alzheimer Research Foundation (SAO-FRA) and the Alzheimer's Association USA. B.D.S. holds the Bax-Vanluffelen Chair for Alzheimer's Disease.

Authors' contributions

L.S., A.Si., E.P., I.G. and B.D.S. conceived and designed the study and wrote the manuscript. L.S., A.Si., E.P., I.G., A.M.M., A.N., A.Sn. performed experiments and analyzed data together with B.D.S. All authors discussed the results and commented on the manuscript.

Data availability

Bulk sequencing data are deposited in the Gene Expression Omnibus (GSE289715) and from the B.D.S. lab website (URL). Mice are deposited to the European Mutant Archive (EMMA). All materials used in the current work can be obtained upon request to B.D.S. and will be made available under the standard MTA of VIB.

Declarations

Ethics approval and consent to participate

All animal experiments were conducted according to protocols approved by the local Ethical Committee of Laboratory Animals of KU Leuven (P125-2022). The use of human ESC (H9) and iPSC (UKBi011-A-3) are approved by the local Ethical Committee of UZ Leuven (S63481).

Consent for publication

Not applicable.

Competing interests

B.D.S. is or has been a consultant for Eli Lilly, Biogen, Janssen Pharmaceutica, Eisai, AbbVie and other companies. B.D.S. is also a scientific founder of Augustine Therapeutics and a scientific founder and stockholder of Muna Therapeutics. I.G. and A.N. are currently employees at Muna Therapeutics.

Received: 15 November 2024 Accepted: 2 March 2025

Published online: 11 March 2025

References

1. Abud EM, Ramirez RN, Martinez ES, Healy LM, Nguyen CHH, Newman SA, Yeromin AV, Scarfone VM, Marsh SE, Fimbres C, Caraway CA, Fote GM, Madany AM, Agrawal A, Kaye R, Gylis KH, Cahalan MD, Cummings BJ, Antel JP, Blurton-Jones M. iPSC-derived human microglia-like cells to study neurological diseases. *Neuron*. 2017;94(2):278-293.e9. <https://doi.org/10.1016/J.NEURON.2017.03.042>.

2. Baligács N, Albertini G, Borrie SC, Serneels L, Pridans C, Balusu S, De Strooper B. Homeostatic microglia initially seed and activated microglia later reshape amyloid plaques in Alzheimer's Disease. *Nat Commun*. 2024;15(1):10634. <https://doi.org/10.1038/S41467-024-54779-W>.
3. Benichou G, Yamada Y, Aoyama A, Madsen JC. Natural killer cells in rejection and tolerance of solid organ allografts. *Curr Opin Organ Transplant*. 2011;16(1):47–53. <https://doi.org/10.1097/MOT.0B013E32834254CF>.
4. Bittencourt SA. (2010). FastQC A Quality Control tool for High Throughput Sequence Data. Babraham Bioinformatics. <http://www.bioinformatics.babraham.ac.uk/projects/fastqc/>
5. Bohlen CJ, Bennett FC, Tucker AF, Collins HY, Mulinyawe SB, Barres BA. Diverse Requirements for Microglial Survival, Specification, and Function Revealed by Defined-Medium Cultures. *Neuron*. 2017;94(4):759–773.e8. <https://doi.org/10.1016/J.NEURON.2017.04.043>.
6. Capotondo A, Milazzo R, Garcia-Manteiga JM, Cavalca E, Montepeloso A, Garrison BS, Peviani M, Rossi DJ, Biffi A. Intracerebroventricular delivery of hematopoietic progenitors results in rapid and robust engraftment of microglia-like cells. *Sci Adv*. 2017;3(12):e1701211. <https://doi.org/10.1126/SCIADV.1701211>.
7. Chadarevian JP, Hasselmann J, Lahian A, Capocchi JK, Escobar A, Lim TE, Le L, Tu C, Nguyen J, Kiani Shabestari S, Carlen-Jones W, Gandhi S, Bu G, Hume DA, Pridans C, Wszolek ZK, Spitale RC, Davtayan H, Blurton-Jones M. Therapeutic potential of human microglia transplantation in a chimeric model of CSF1R-related leukoencephalopathy. *Neuron*. 2024;112(16):2686–2707.e8. <https://doi.org/10.1016/J.NEURON.2024.05.023>.
8. Chadarevian, J. P., Lombroso, S. I., Peet, G. C., Hasselmann, J., Tu, C., Marzan, D. E., Capocchi, J., Purnell, F. S., Nemeč, K. M., Lahian, A., Escobar, A., England, W., Chaluvaadi, S., O'Brien, C. A., Yaqoob, F., Aisenberg, W. H., Porras-Paniagua, M., Bennett, M. L., Davtayan, H., ... Chris Bennett, F. (2023). Engineering an inhibitor-resistant human CSF1R variant for microglia replacement. *The Journal of Experimental Medicine*, 220(3). <https://doi.org/10.1084/JEM.20220857>
9. Claes C, Danhash EP, Hasselmann J, Chadarevian JP, Shabestari SK, England WE, Lim TE, Hidalgo JLS, Spitale RC, Davtayan H, Blurton-Jones M. Plaque-associated human microglia accumulate lipid droplets in a chimeric model of Alzheimer's disease. *Mol Neurodegen*. 2021;16(1):50. <https://doi.org/10.1186/S13024-021-00473-0>.
10. Claes C, England WE, Danhash EP, Kiani Shabestari S, Jairaman A, Chadarevian JP, Hasselmann J, Tsai AP, Coburn MA, Sanchez J, Lim TE, Hidalgo JLS, Tu C, Cahalan MD, Lamb BT, Landreth GE, Spitale RC, Blurton-Jones M, Davtayan H. The P522R protective variant of PLCG2 promotes the expression of antigen presentation genes by human microglia in an Alzheimer's disease mouse model. *Alzheimer's & Dementia : The Journal of the Alzheimer's Association*. 2022;18(10):1765–78. <https://doi.org/10.1002/ALZ.12577>.
11. Deczkowska A, Keren-Shaul H, Weiner A, Colonna M, Schwartz M, Amit I. Disease-Associated Microglia: A Universal Immune Sensor of Neurodegeneration. *Cell*. 2018;173(5):1073–81. <https://doi.org/10.1016/J.CELL.2018.05.003>.
12. Dobin A, Davis CA, Schlesinger F, Drenkow J, Zaleski C, Jha S, Batut P, Chaisson M, Gingeras TR. STAR: ultrafast universal RNA-seq aligner. *Bioinformatics (Oxford, England)*. 2013;29(1):15–21. <https://doi.org/10.1093/BIOINFORMATICS/BTS635>.
13. Dolan MJ, Therrien M, Jereb S, Kamath T, Gazestani V, Atkeson T, Marsh SE, Goeva A, Lojek NM, Murphy S, White CM, Joung J, Liu B, Limone F, Eggan K, Hacohen N, Bernstein BE, Glass CK, Leinonen V, Stevens B. Exposure of iPSC-derived human microglia to brain substrates enables the generation and manipulation of diverse transcriptional states in vitro. *Nature Immunol*. 2023;24(8):1382–90. <https://doi.org/10.1038/S41590-023-01558-2>.
14. Fabriek, B. O., Van Haastert, E. S., Galea, I., Polfliet, M. M. J., Opp, E. D. D. E., Van Den Heuvel, M. M., Van Den Berg, T. K., De Groot, C. J. A., Van Der Valk, P., & Dijkstra, C. D. (2005). CD163-Positive Perivascular Macrophages in the Human CNS Express Molecules for Antigen Recognition and Presentation. 51 (glia), 297–305. <https://doi.org/10.1002/glia.20208>
15. Fattorelli N, Martinez-Muriana A, Wolfs L, Geric I, De Strooper B, Mancuso R. Stem-cell-derived human microglia transplanted into mouse brain to study human disease. *Nat Protoc*. 2021;16(2):1013–33. <https://doi.org/10.1038/S41596-020-00447-4>.
16. Felsky, D., Roostaei, T., Nho, K., Risacher, S. L., Bradshaw, E. M., Petyuk, V., Schneider, J. A., Saykin, A., Bennett, D. A., & De Jager, P. L. (2019). Neuropathological correlates and genetic architecture of microglial activation in elderly human brain. *Nat Commun* 2019 10:1, 10(1), 1–12. <https://doi.org/10.1038/s41467-018-08279-3>
17. Geirsdottir L, David E, Keren-Shaul H, Weiner A, Bohlen SC, Neuber J, Balic A, Giladi A, Sheban F, Dutertre CA, Pfeifle C, Peri F, Raffo-Romero A, Vizioli J, Matiassek K, Scheiwe C, Meckel S, Mätz-Rensing K, van der Meer F, Prinz M. Cross-species single-cell analysis reveals divergence of the primate microglia program. *Cell*. 2019;179(7):1609–1622.e16. <https://doi.org/10.1016/J.CELL.2019.11.010>.
18. Gosselin D, Skola D, Coufal NG, Holtman IR, Schlachetzki JCM, Sajti E, Jaeger BN, O'Connor C, Fitzpatrick C, Pasillas MP, Pena M, Adair A, Gonda DD, Levy ML, Ransohoff RM, Gage FH, Glass CK. An environment-dependent transcriptional network specifies human microglia identity. *Science*. 2017;356(6344):1248–59. <https://doi.org/10.1126/SCIENCE.AAL3222>.
19. Harris SE, MacDougall M, Horn D, Woodruff K, Zimmer SN, Rebel VI, Fajardo R, Feng JQ, Gluhak-Heinrich J, Harris MA, Abboud Werner S. Meox2Cre-mediated Disruption of CSF-1 Leads to Osteopetrosis and Osteocyte Defects. *Bone*. 2012;50(1):42. <https://doi.org/10.1016/J.BONE.2011.09.038>.
20. Hasselmann J, Coburn MA, England W, Figueroa Velez DX, Kiani Shabestari S, Tu CH, McQuade A, Kolahdouzan M, Echeverria K, Claes C, Nakayama T, Azevedo R, Coufal NG, Han CZ, Cummings BJ, Davtayan H, Glass CK, Healy LM, Gandhi SP, Blurton-Jones M. Development of a Chimeric model to study and manipulate human microglia in vivo. *Neuron*. 2019;103(6):1016–1033.e10. <https://doi.org/10.1016/j.neuron.2019.07.002>.
21. Huang DW, Sherman BT, Lempicki RA. Systematic and integrative analysis of large gene lists using DAVID bioinformatics resources. 2008. <https://doi.org/10.1038/nprot.2008.211>.
22. Keren-Shaul H, Spinrad A, Weiner A, Matcovitch-Natan O, Dvir-Szternfeld R, Ulland TK, David E, Baruch K, Lara-Astasio D, Toth B, Itzkovitz S, Colonna M, Schwartz M, Amit I. A Unique Microglia Type Associated with Restricting Development of Alzheimer's Disease. *Cell*. 2017;169(7):1276–1290.e17. <https://doi.org/10.1016/J.CELL.2017.05.018>.
23. Kondo M, Weissman IL, Akashi K. Identification of clonogenic common lymphoid progenitors in mouse bone marrow. *Cell*. 1997;91(5):661–72. [https://doi.org/10.1016/S0092-8674\(00\)80453-5](https://doi.org/10.1016/S0092-8674(00)80453-5).
24. Krasemann S, Madore C, Cialic R, Baufeld C, Calcagno N, El Fatimy R, Beckers L, O'Loughlin E, Xu Y, Fanek Z, Greco DJ, Smith ST, Tweet G, Humulock Z, Zrzavy T, Conde-Sanroman P, Gacias M, Weng Z, Chen H, Butovsky O. The TREM2-APOE pathway drives the transcriptional phenotype of dysfunctional microglia in neurodegenerative diseases. *Immunity*. 2017;47(3):566–581.e9. <https://doi.org/10.1016/J.IMMUNI.2017.08.008>.
25. Kwon OJ, Zhang B, Jia D, Zhang L, Wei X, Zhou Z, Liu D, Huynh KT, Zhang K, Zhang Y, Labhart P, Sboner A, Barbieri C, Haffner MC, Creighton CJ, Xin L. Elevated expression of the colony-stimulating factor 1 (CSF1) induces prostatic intraepithelial neoplasia dependent of epithelial-Gp130. *Oncogene*. 2022;41(9):1309–23. <https://doi.org/10.1038/S41388-021-02169-7>.
26. Li Q, Barres BA. Microglia and macrophages in brain homeostasis and disease. *Nat Rev Immunol*. 2018;18(4):225–42. <https://doi.org/10.1038/NRI.2017.125>.
27. Liao Y, Smyth GK, Shi W. featureCounts: an efficient general purpose program for assigning sequence reads to genomic features. *Bioinformatics*. 2014;30(7):923–30. <https://doi.org/10.1093/BIOINFORMATICS/BTT656>.
28. Mancuso R, Fattorelli N, Martinez-Muriana A, Davis E, Wolfs L, Van Den Daele J, Geric I, Premereur J, Polanco P, Bijnens B, Preman P, Serneels L, Poovathingal S, Balusu S, Verfaillie C, Fiers M, De Strooper B. Xenografted human microglia display diverse transcriptomic states in response to Alzheimer's disease-related amyloid- β pathology. *Nat Neurosci*. 2024;27(5):886–900. <https://doi.org/10.1038/s41593-024-01600-y>.
29. Mancuso R, Van Den Daele J, Fattorelli N, Wolfs L, Balusu S, Burton O, Liston A, Sierksma A, Fourné Y, Poovathingal S, Arranz-Mendiguren A, Sala Frigerio C, Claes C, Serneels L, Theys T, Perry VH, Verfaillie C, Fiers M, De Strooper B. Stem-cell-derived human microglia transplanted in mouse brain to study human disease. *Nat Neurosci*. 2019;22(12):2111–6. <https://doi.org/10.1038/S41593-019-0525-X>.
30. McQuade A, Coburn M, Tu CH, Hasselmann J, Davtayan H, Blurton-Jones M. Development and validation of a simplified method to generate human microglia from pluripotent stem cells. *Mol Neurodegen*. 2018;13(1):67. <https://doi.org/10.1186/S13024-018-0297-X>.
31. Mittelbronn M, Dietz K, Schluesener HJ, Meyermann R. Local distribution of microglia in the normal adult human central nervous system differs

- by up to one order of magnitude. *Acta Neuropathol.* 2001;101(3):249–55. <https://doi.org/10.1007/S004010000284/METRICS>.
32. Munro DAD, Bestard-Cuche N, McQuaid C, Chagnot A, Shabestari SK, Chadarevian JP, Maheshwari U, Szymkowiak S, Morris K, Mohammad M, Corsinotti A, Bradford B, Mabbott N, Lennen RJ, Jansen MA, Pridans C, McColl BW, Keller A, Blurton-Jones M, Priller J. Microglia protect against age-associated brain pathologies. *Neuron.* 2024;112(16):2732–2748.e8. <https://doi.org/10.1016/J.NEURON.2024.05.018>.
 33. Nimmerjahn A, Kirchhoff F, Helmchen F. Resting microglial cells are highly dynamic surveillants of brain parenchyma in vivo. *Science (New York, NY).* 2005;308(5726):1314–8. <https://doi.org/10.1126/SCIENCE.1110647>.
 34. Rathinam C, Poueymirou WT, Rojas J, Murphy AJ, Valenzuela DM, Yancopoulos GD, Rongvaux A, Eynon EE, Manz MG, Flavell RA. Efficient differentiation and function of human macrophages in humanized CSF-1 mice. *Blood.* 2011;118(11):3119–28. <https://doi.org/10.1182/BLOOD-2010-12-326926>.
 35. Roh YJ, Gong JE, Kim JE, Jin YJ, Song HJ, Seol A, Park J, Lim Y, Hwang DY. Comparison of immunophenotypes between Rag2 knockout mice derived from two different sources. *Lab Anim Res.* 2023;39(1):2. <https://doi.org/10.1186/S42826-023-00153-8>.
 36. Rojo R, Raper A, Ozdemir DD, Lefevre L, Grabert K, Wollscheid-Lengeling E, Bradford B, Caruso M, Gazova I, Sánchez A, Lisowski ZM, Alves J, Molina-Gonzalez I, Davtyan H, Lodge RJ, Glover JD, Wallace R, Munro DAD, David E, Pridans C. Deletion of a Csf1r enhancer selectively impacts CSF1R expression and development of tissue macrophage populations. *Nat Commun.* 2019;10(1):3215. <https://doi.org/10.1038/S41467-019-11053-8>.
 37. Saito T, Matsuba Y, Mihira N, Takano J, Nilsson P, Itohara S, Iwata N, Saido TC. Single App knock-in mouse models of Alzheimer's disease. 2014. <https://doi.org/10.1038/nn.3697>.
 38. Sala Frigerio C, Wolfs L, Fattorelli N, Thrupp N, Voytyuk I, Schmidt I, Mancuso R, Chen WT, Woodbury ME, Srivastava G, Möller T, Hudry E, Das S, Saido T, Karran E, Hyman B, Perry VH, Fiers M, De Strooper B. The major risk factors for Alzheimer's disease: age, sex, and genes modulate the microglia response to A β plaques. *Cell Rep.* 2019;27(4):1293–1306.e6. <https://doi.org/10.1016/J.CELREP.2019.03.099>.
 39. Sankowski R, Süß P, Benkendorff A, Böttcher C, Fernandez-Zapata C, Chhatbar C, Cahueau J, Monaco G, Gasull AD, Khavaran A, Grauvogel J, Scheiwe C, Shah MJ, Heiland DH, Schnell O, Markfeld-Erol F, Kunze M, Zeiser R, Priller J, Prinz M. Multiomic spatial landscape of innate immune cells at human central nervous system borders. *Nat Med.* 2023;30(1):186–98. <https://doi.org/10.1038/s41591-023-02673-1>.
 40. Serneels L, T'Syen D, Perez-Benito L, Theys T, Holt MG, De Strooper B. Modeling the β -secretase cleavage site and humanizing amyloid-beta precursor protein in rat and mouse to study Alzheimer's disease. *Mol Neurodegen.* 2020;15(1):60. <https://doi.org/10.1186/S13024-020-00399-Z>.
 41. Shinkai Y, Rathbun, OGary, Lam, K. P., Oltz, E. M., Stewart, V., Mendelsohn, M., Charon, J., Datta, M., Young, F., Stall, A. M., Alt, F. W. RAG-2-deficient mice lack mature lymphocytes owing to inability to initiate V(D)J rearrangement. *Cell.* 1992;68(5):855–67. [https://doi.org/10.1016/0092-8674\(92\)90029-C](https://doi.org/10.1016/0092-8674(92)90029-C).
 42. Shultz LD, Ishikawa F, Greiner DL. Humanized mice in translational biomedical research. *Nat Rev Immunol.* 2007;7(2):118–30. <https://doi.org/10.1038/NRI2017>.
 43. Svoboda DS, Barrasa MI, Shu J, Rietjens R, Zhang S, Mitalipova M, Berube P, Fu D, Shultz LD, Bell GW, Jaenisch R. Human iPSC-derived microglia assume a primary microglia-like state after transplantation into the neonatal mouse brain. *Proc Natl Acad Sci USA.* 2019;116(50):25293–303. <https://doi.org/10.1073/PNAS.1913541116>.
 44. Todd BP, Chimenti MS, Luo Z, Ferguson PJ, Bassuk AG, Newell EA. Traumatic brain injury results in unique microglial and astrocyte transcriptomes enriched for type I interferon response. *J Neuroinflammation.* 2021;18(1):1–15. <https://doi.org/10.1186/S12974-021-02197-W/FIGURES/9>.
 45. Tuddenham, J. F., Taga, M., Haage, V., Marshe, V. S., Roostaei, T., White, C., Lee, A. J., Fujita, M., Khairallah, A., Zhang, Y., Green, G., Hyman, B., Frosch, M., Hopp, S., Beach, T. G., Serrano, G. E., Corboy, J., Habib, N., Klein, H.-U., ... De Jager, P. L. (2024). A cross-disease resource of living human microglia identifies disease-enriched subsets and tool compounds recapitulating microglial states. *Nature Neuroscience* 2024, 1–17. <https://doi.org/10.1038/s41593-024-01764-7>.
 46. Ueno M, Fujita Y, Tanaka T, Nakamura Y, Kikuta J, Ishii M, Yamashita T. Layer V cortical neurons require microglial support for survival during postnatal development. *Nat Neurosci.* 2013;16(5):543–51. <https://doi.org/10.1038/NN.3358>.
 47. van den Bosch AMR, van der Poel M, Fransen NL, Vincenent MCJ, Bobeldijk AM, Jongejan A, Engelenburg HJ, Moerland PD, Smolders J, Huitinga I, Hamann J. Profiling of microglia nodules in multiple sclerosis reveals propensity for lesion formation. *Nat Commun.* 2024;15(1):1–16. <https://doi.org/10.1038/s41467-024-46068-3>.
 48. Xia D, Lianoglou S, Sandmann T, Calvert M, Suh JH, Thomsen E, Dugas J, Pizzo ME, DeVos SL, Earr TK, Lin CC, Davis S, Ha C, Leung AWS, Nguyen H, Chau R, Yulyaningsih E, Lopez I, Solano H, Sanchez PE. Novel App knock-in mouse model shows key features of amyloid pathology and reveals profound metabolic dysregulation of microglia. *Mol Neurodegen.* 2022;17(1):41. <https://doi.org/10.1186/S13024-022-00547-7>.
 49. Xu R, Li X, Boreland AJ, Posyton A, Kwan K, Hart RP, Jiang P. Human iPSC-derived mature microglia retain their identity and functionally integrate in the chimeric mouse brain. *Nat Commun.* 2020;11(1):1–16. <https://doi.org/10.1038/s41467-020-15411-9>.
 50. Yin Z, Rosenzweig N, Kleemann KL, Zhang X, Brandão W, Margeta MA, Schroeder C, Sivanathan KN, Silveira S, Gauthier C, Mallah D, Pitts KM, Durao A, Herron S, Shorey H, Cheng Y, Barry JL, Krishnan RK, Wakelin S, Butovsky O. APOE4 impairs the microglial response in Alzheimer's disease by inducing TGF β -mediated checkpoints. *Nat Immunol.* 2023;24(11):1839–53. <https://doi.org/10.1038/S41590-023-01627-6>.
 51. Yoshida H, Hayashi S-L, Kunisada T, Ogawa M, Nishikawa S, Okamura H, Sudo T, Shultz LD, Nishikawa S-L. The murine mutation osteopetrosis is in the coding region of the macrophage colony stimulating factor gene. *Lett Nat.* 1990;348:442.

Publisher's Note

Springer Nature remains neutral with regard to jurisdictional claims in published maps and institutional affiliations.